34.0 PHASE AND TEXTURE EVOLUTION PRECEDING ABNORMAL GRAIN GROWTH IN NI-BASED AEROSPACE ALLOYS

Byron McArthur (Mines)
Faculty: Amy Clarke (Mines), Michael Kaufman (Mines) and Kester Clarke (Mines)
Industrial Mentors: Eric Payton (AFRL), Kevin Severs (ATI)

This project initiated in Fall 2017 and is advised by Amy Clarke, Michael Kaufman and Kester Clarke at Colorado School of Mines (Mines). The research performed during this project will serve as the basis for a Ph.D. thesis for Byron McArthur.

Project Overview and Industrial Relevance

Nickel-based superalloys are utilized extensively in the aerospace industry for their excellent high temperature strength, fatigue life, oxidation resistance and corrosion resistance. Turbine engine discs are flight critical components, and failure of these components risks loss of the entire aircraft. With the continuous push for more efficient commercial aviation, higher operating temperatures and pressures are desired. Complex Ni-based superalloys are being processed through novel methods to meet these stringent requirements [34.1].

The alloy investigated in the present study is RR1000, a γ-γ' disk alloy with approximately 45% volume fraction of γ' at room temperature. Processing steps for this alloy include alloyed powderization, hot isostatic pressing, and extrusion at a 4.5:1 reduction ratio [34.1]. These steps produce a fully dense, recrystallized billet with γ grain size of 1-5 µm diameter and a distribution of primary γ' (γ_1', 1-3 µm) and secondary γ' (γ_2', 20-50 nm). Two material conditions provided are shown in **Figure 34.1**; note the significant difference in fraction of γ_1'. Subsequent isothermal deformation processing of slices of material is performed near the γ' solvus temperature; γ_2' is dissolved while γ_1' pins the γ grain boundaries and superplastic deformation keeps flow stresses low. Super-solvus heat treatment (SSHT), performed after isothermal forging, allows for γ growth to approximately 50 µm for increased creep resistance during service [34.1]. Abnormal grain growth (AGG) has been shown to occur during the SSHT step, and varies based upon processing parameters during the isothermal deformation (ε, $\dot{\varepsilon}$, T) and the SSHT heating rate. AGG can result in γ grains up to 3 mm that compromise mechanical performance and are difficult to detect via non-destructive testing. The objective of this project is to better understand the microstructural mechanisms that cause AGG in these materials.

Previous Work

34.1.1 Literature Review

Prior research into AGG has been most successful in exploring the processing parameters required to produce AGG in an effort to prevent the phenomena from occurring in industrial settings. Huron et al. [34.2] performed double cone isothermal compression testing on a similar alloy (René 88DT) and found a range of strain rates and deformation temperatures that produce AGG; increasing deformation temperature required higher strain rates to produce AGG. Parr et al. [34.3] did similar testing on RR1000 and found AGG conditions to occur at near-γ'-solvus deformation temperatures, low strain rates, and low strains; similar to those explored in the present study. In-depth work performed by Payton [34.4] explored characterization techniques in an effort to understand the microstructural mechanism behind AGG; results indicated stored energy within the γ grains was a likely contributor to AGG, however combined contributions from γ' coherency changes and redistribution are important as well.

Work further exploring the AGG mechanisms has been performed by Charpagne et al. [34.5], and proposes that stored energy is the driving force for AGG, with static recrystallization of γ grains initiating the process. The recrystallization of the γ grains has been proposed by Charpagne to occur coherently off of γ_1', followed by growth to consume neighboring regions containing stored energy; this mechanism has been termed 'heteroepitaxial recrystallization' (HERX). Coherency reduces the energy barrier for recrystallization of γ, theoretically allowing it to occur at lower temperatures. Interestingly, γ grain boundaries appear to pass through large γ_1' with relatively low Zener pinning influence. Charpagne's work demonstrated continued growth of γ grains within critical regions until impingement upon each other limited grain growth. This suggests final grain size is determined by the number and distribution of nucleation sites that then grow to consume regions of unrecrystallized grains.

34.1.2 Thermomechanical Processing to Produce Abnormal Grain Growth

Prior experiments in this study focused on establishing the thermomechanical processing parameters for consistently producing AGG in the experimental RR1000 materials. The main portion of this research is focused on the material with the starting condition shown in **Figure 34.1a**, containing a lower fraction of γ_1', smaller γ_2' and larger γ grains, as this material has shown instances of AGG during testing. Isothermal compression of RR1000 specimens was performed in a Gleeble® thermomechanical simulator, enabling control of deformation temperature, strain, and strain rate as well as providing load-displacement data. Post-deformation SSHT of the material was performed in a TA Instruments quenching dilatometer to maintain precise temperature and heating rate control, as well as measure qualitative γ' dissolution and γ grain growth behavior via dilation. The deformation temperature, strain rate, and strain that produced AGG were 1110°C, 0.0008 ε/s and 0.16 ε, respectively, just below the 1135-1145°C γ' solvus temperature. In dilatometry, a low heating rate (0.12°C/s) up to the SSHT temperature (1170°C) promoted AGG occurrence.

The results from the present study support a mechanism akin to the HERX mechanism previously described. although the origins of the nuclei that lead to AGG remain uncertain. Deformation during isothermal forging imparts a stored energy that may provide the driving force for specific nuclei to grow and result in AGG, yet is insufficient for traditional, homogeneous recrystallization. The slow heating rate during SSHT may result in recovery in the γ and slow dissolution of the γ_1' to form stable AGG nuclei. The γ_1' phase fraction, size, and distribution appear to be of importance, as observed from the sensitivity of the two starting conditions of material to creating AGG. While the γ_2' are dissolved at isothermal forging and heat treating temperatures, the γ_1' remains and serves as AGG nucleation sites.

Recent Progress

34.1.3 Pseudo-in-situ Interrupted Heat Treatments

Interrupted heat treatments of RR1000 to track AGG proved difficult due to the statistical nature of observing a nucleation site in a 2-D plane of 3-D material. Instead of processing the material to create AGG, which would have rare recrystallization nuclei, deformation and heat treatments were selected to create numerous incoherent γ_1'. Initially, the as-received state was utilized, however extensive multi-micrometer coherent γ_1' already existed in γ grains, as shown in **Figure 34.2**. This has previously been reported in the literature [34.6] for material in a similar condition the as-received material in the present study, and was likely due to dynamic or metadynamic recrystallization during prior thermomechanical processing, very similar to the current mechanism being discussed and investigated. To create a more ideal starting material prior to room temperature deformation, sub-γ' solvus heat treatments (1110-1130°C) were performed to reduce the amount of coherent γ_1' by dissolving some and allowing for competitive γ boundary movement to consume γ shells surrounding γ_1'. Deformed specimens were heat treated in an argon back filled vacuum dilatometer to specified temperatures and specified heating rates, then argon quenched, polished and analyzed using a scanning electron microscope (SEM) equipped with an electron back scatter diffraction (EBSD) detector. The heat treatment continued on the same sample at the interrupted point to the next specified temperature, followed by repeated SEM preparation and analysis of the same location on the specimen. Final microstructures were compared to uninterrupted and post-treatment sectioning, confirming the interrupted experimental conditions did not change the final microstructures.

The microstructural evolution during the heat treatment is tracked from the as-deformed state through sub-γ' solvus heat treatments of 1050°C, 1075°C, and 1100°C. As hypothesized, an incoherent γ_1' nucleated a coherent, strain free γ that grew to consume neighboring γ, as shown in **Figure 34.3**. The grain reference orientation deviation (GROD) maps for the corresponding temperatures, **Figure 34.4**, indicate stored energy within the grain bulk, evident by geometrically necessary dislocations causing internal misorientations. These GROD maps demonstrate the reduction in stored energy by growth of the nucleated, strain free γ grains during the interrupted heat treatment. Small γ grains adjacent to γ_1' appear to be consumed by coherent γ at temperatures lower than 1075°C, likely driven by the reduction in high angle grain boundaries and their high mobility. Between 1075 and 1100°C, larger γ grains with stored energy are rapidly consumed by recrystallized, strain free γ. This is likely due to continued dissolution of γ_2' combined with higher boundary mobility. These boundaries are able to pass by γ_1' to consume neighboring γ (if they contain stored energy), change the γ_1' to intragranular, incoherent γ_1' in the process, regardless of the previous γ_1' orientation. Interestingly, during the microstructural evolution (other than pinning unrecrystallized γ grain boundaries) coherent

γ_1' played no significant role, nor differed much from intergranular incoherent γ_1'. The γ_1' sometimes demonstrated rotation when at γ boundaries or with γ boundary transmission during grain growth.

34.1.4 Observing Interfaces via Diffusion Bonding

Diffusion bonding of numerous alloys was attempted through multiple techniques. A dilatometer with 10^{-6} Torr vacuum and compressive load was expected to prevent a significant oxide barrier and to allow for diffusion. The Gleeble® system uses resistive heating and an applied load, and was also expected to break through any oxide barrier. These efforts worked with nickel bonded to a nickel-aluminum alloy of stoichiometric Ni_3Al composition, as presented in the Spring 2020 CANFSA report and Summer 2020 CANFSA video conference; however, Ni-based superalloys' combined chromium, aluminum, titanium, and halfnium created oxides that proved impenetrable by diffusion at the desired processing temperatures. A gas mixture of ~4% hydrogen in argon or nitrogen is expected to possibly alleviate this issue; however, limitations on introducing hydrogen into either equipment prevented our use of this technique.

Plans for Next Reporting Period

Upcoming efforts will continue with interrupted heat treatment experiments, aimed at two goals: 1) Providing additional understanding and evidence of an HERX based mechanism creating AGG, and 2) Exploring industrially feasible methods of alleviating AGG. The first goal will be investigated with an increased heat treatment temperature prior to deformation (1130°C instead of 1110°C), and an additional hold time may be added to allow for γ grain growth to reduce coherent γ_1' without significantly reducing overall γ_1' fraction. The second goal will be addressed through modifications to thermomechanical processing and heat treating while recognizing workpiece thermal mass and maximum die load limitations.

References

[34.1]   M. C. Hardy, B. Zirbel, G. Shen, R. Shankar. Developing damage tolerance and creep resistance in a high strength nickel alloy for disc applications, Superalloys 2004 83 (2004).

[34.2]   E. Raymond, E. Huron, S. Srivasta. Control of grain size via forging strain rate rimits for R'88DT, Superalloys 49 (2000).

[34.3]   I. M. D. Parr, T. J. Jackson, M. C. Hardy, D. J. Child, C. Argyrakis, K. Severs, V. Saraf, J. M. Stumpf. Inhomogeneous grain coarsening behavior in supersolvus heat treated nickel-based superalloys RR1000, Superalloys 447 (2016).

[34.4]   E. J. Payton, Characterization and modeling of grain coarsening in powder metallurgical nickel-based superalloys, The Ohio State University (2009).

[34.5]   M. A. Charpagne, J. M. Franchet, N. Bozzolo. Overgrown grains appearing during sub-solvus heat treatment in a polycrystalline γ-γ' Nickel-based superalloy, Mater. Des. 144, 353 (2018).

[34.6]   M.A. Charpagne, P. Vennegues, T. Billot, J.M. Franchet, N. Bozzolo. Evidence of multimicrometric coherent γ' precipitates in a hot-forged γ–γ' nickel-based superalloy, J. Microsc. 263 (2016).
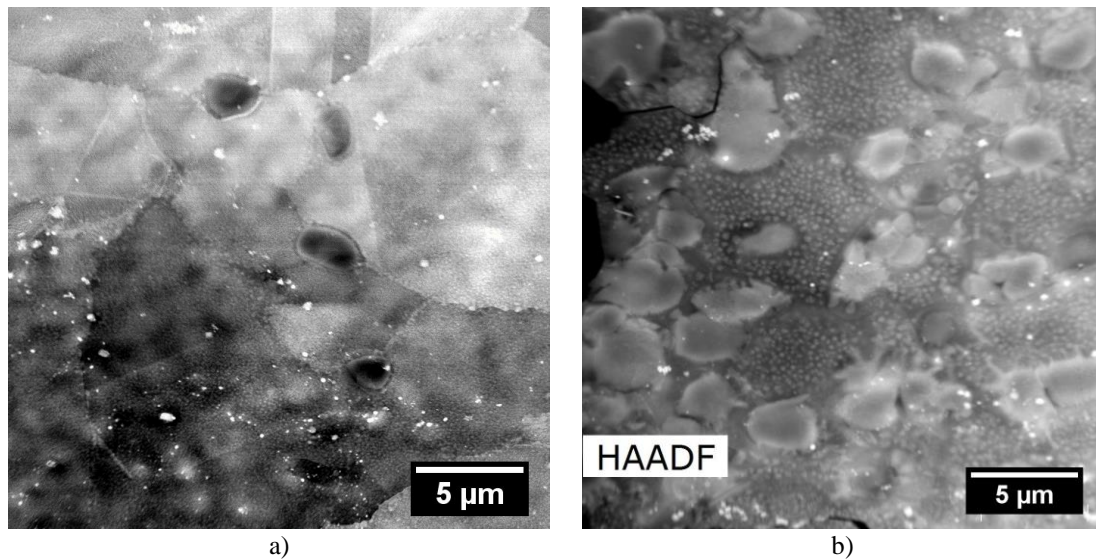
Figures and Tables

Figure 34.1: TEM micrographs of starting material conditions for 'Slice' 1 (a) and 2 (b) in Bright Field (BF) and High Angle Anular Dark Field (HAADF) imaging modes, respectively. Slice 1 has γ_1' shown in darker regions, with γ_2'dispersed throughout the γ grains. Slice 2 shows higher volume fraction of γ_1' and larger γ_2'. Note the lighter regions are likely carbides and halfnia clusters remaining in the material as well as redeposited during electropolishing (Images courtesy of Yaofeng Gao, Mines).
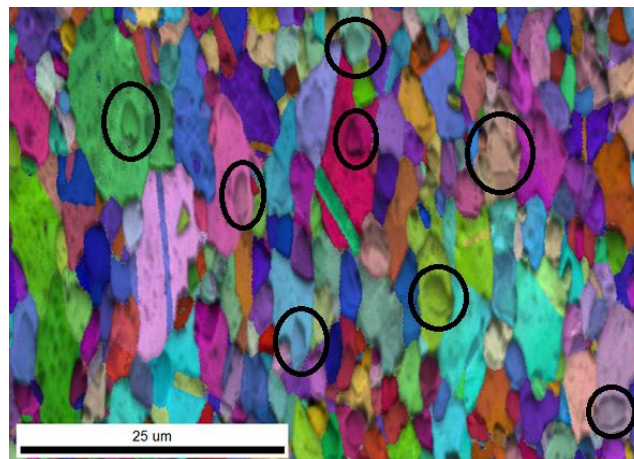

Figure 34.2: SEM-EBSD orientation map and image quality overlay of as-received material ('Slice 1'). Note the γ_1' coherent within the γ matrix in black circles.
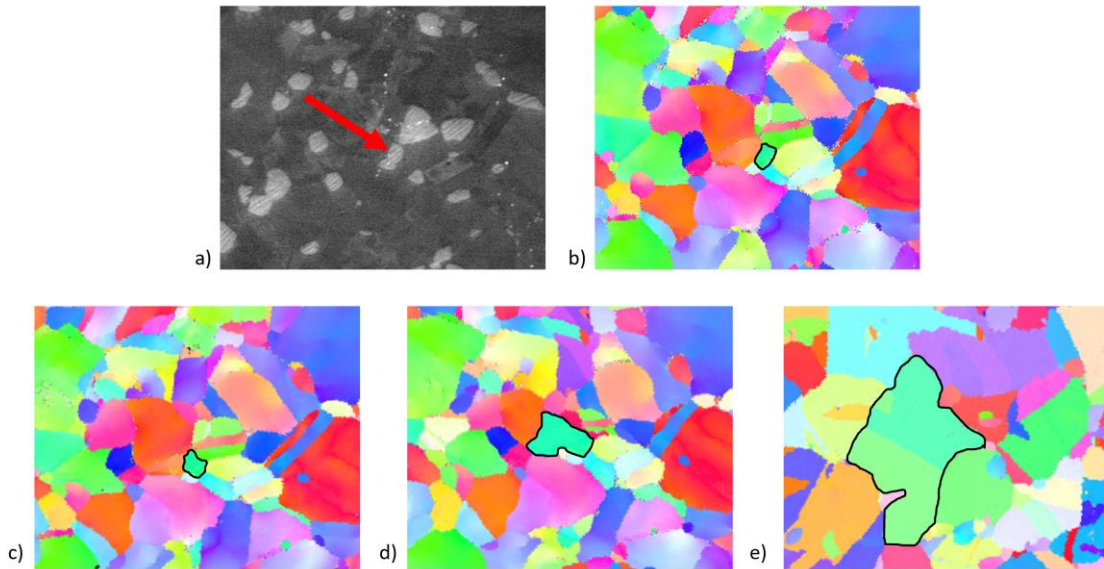
34.4

Figure 34.3: (a) SEM-SEI Micrograph for a specimen compressed to 15% height reduction, and (b) SEM-EBSD orientation map. SEM-EBSD orientation maps of the same region heat treated to (c) 1050°C, (d) 1075°C and (e) 1100°C. Note the γ_1' indicated by a red arrow (a) and black outline (b), with subsequent γ recrystallization growth with black outline in (c), (d) and (e). An annealing twin is visible in orientation map (e).
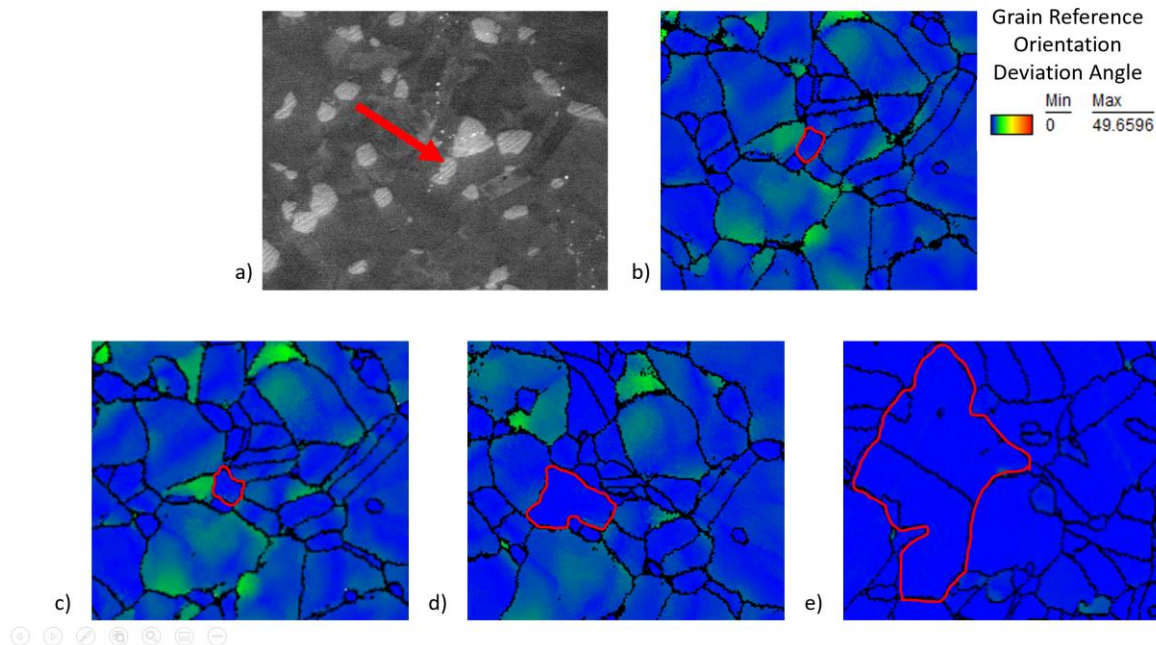

Figure 34.4: The same region as Figure 34.3, with (a) SEM-SEI Micrograph for a specimen compressed to 15% height reduction , and (b) SEM-GROD map. SEM-GROD maps of the same region heat treated to (c) 1050°C, (d) 1075°C and (e) 1100°C. Note the γ_1' indicated by a red arrow (a) and red outline (b), with subsequent γ recrystallization growth with red outline in (c), (d) and (e).

34.5